Effect of Multi-Component Nanocomposites on the Anti-Aging Performance of Asphalt

Genfu LIANG[1], Linghai KONG[1], A Gudamu[1], Xunlin He[1], and Chongzheng ZHU [2*]

[1] CCCC Third Highway Engineering Co., Ltd. Third Engineering Company, Wuhan 430033, China
[2] College of Civil Engineering, Xiangtan University, Xiangtan 411105, China
[*] Corresponding author. E-mail: zhuchongzheng@xtu.edu.cn

Received: Jun. 23, 2026; Accepted: Aug. 18, 2026

To improve the aging resistance of asphalt, two multi-component nanocomposites, titanium dioxide/montmorillonite (TM) and cerium oxide/montmorillonite (CM), were prepared using the sol-gel method. Corresponding modified asphalts (TMMA and CMMA) were fabricated via melt blending. Field emission scanning electron microscopy (FE-SEM) and ultraviolet-visible absorption spectroscopy (UV-Vis) characterized the microstructure and optical properties of the nanocomposites. Thermal-oxidative and ultraviolet aging were simulated using the rolling thin film oven test (RTFOT), pressure aging vessel (PAV), and ultraviolet accelerated aging test. Physical, rheological and chemical property changes of the modified asphalts were systematically evaluated. FE-SEM revealed that nano- TiO_2 was uniformly loaded on MMT in TM, whereas nano- CeO_2 tended to agglomerate in CM. UV-Vis showed TM had markedly higher ultraviolet absorbance than CM. Before aging, the addition of appropriate nanocomposite improved low-temperature ductility and consistency. After PAV and UV aging, both modified asphalts exhibited lower softening point increments, complex modulus aging indexes and carbonyl index increments than base asphalt, with 2% TMMA outperforming 2% CMMA. Results demonstrate that TM and CM effectively retard thermal-oxidative and ultraviolet aging through possible combined effects of MMT's layered physical barrier and the ultraviolet shielding/antioxidant properties of nano- TiO_2 or nano- CeO_2.

Keywords: modified asphalt; titanium dioxide/montmorillonite nanocomposite; cerium oxide/montmorillonite nanocomposite; anti-aging performance

© The Author('s). This is an open-access article distributed under the terms of the Creative Commons Attribution License (CC BY 4.0), which permits unrestricted use, distribution, and reproduction in any medium, provided the original author and source are cited.

http://dx.doi.org/10.6180/jase.202612_35.066

1. Introduction

Superior road performance has led to the widespread utilization of asphalt pavements. However, during service, asphalt inevitably undergoes changes caused by environmental factors such as heat, oxygen, and ultraviolet (UV) radiation, leading to hardening and embrittlement, which in turn induce cracking, rutting, and other distresses, considerably reducing the lifespan of pavements [1, 2]. Therefore, enhancing the aging resistance of asphalt materials has emerged as a key research priority in the field of pavement engineering.

Asphalt aging is mainly divided into two categories: thermal-oxidative aging and UV aging [3, 4]. Thermo-oxidative aging takes place throughout the construction and in-service phases of asphalt pavements, mainly reflected in the evaporation of lightweight fractions and oxidative reactions. UV aging mainly affects the surface layer of asphalt, triggering photo-oxidation reactions that generate polar oxygen-containing groups such as carbonyls and sulfoxides. These two aging mechanisms often coexist and promote each other, posing a serious challenge to the durability of asphalt pavements.

Table 1. Nomenclature

Abbreviation	Full form
CM	cerium oxide/montmorillonite nanocomposite
CMAI	complex modulus aging index
CMMA	cerium oxide/montmorillonite nanocomposite modified asphalt
DRR	ductility retained rate
FE-SEM	field emission scanning electron microscopy
MMT	montmorillonite
PAV	pressure aging vessel
RP	retained penetration
RTFOT	rolling thin film oven test
SPI	softening point increment
FTIR	Fourier transform infrared spectroscopy
CI	carbonyl index
TM	titanium dioxide/montmorillonite nanocomposite
TMMA	titanium dioxide/montmorillonite nanocomposite modified asphalt
UV	ultraviolet
UV-Vis	ultraviolet-visible absorption spectroscopy

To retard asphalt aging, researchers have attempted to add various anti-aging agents to asphalt. According to their mechanisms of action, anti-aging agents can be mainly classified into UV shielding/absorbing agents, antioxidants, and physical barrier materials [5–7]. With the development of nanotechnology, nanomaterials exhibit unique advantages in asphalt anti-aging modification because of their small size effect and surface effect. Nano-titanium dioxide (TiO_2) possesses outstanding ultraviolet-light absorbing performance and is widely used for UV aging resistance modification of asphalt. Nano-cerium oxide (CeO_2), owing to its abundant oxygen vacancies and free radical scavenging ability, exhibits outstanding antioxidant performance [8]. Two-dimensional nanomaterial montmorillonite (MMT), with its typical layered structure, can effectively delay the penetration of oxygen and heat, thereby inhibiting the thermal-oxidative aging process [9].

However, individual nanomaterials still have certain limitations in asphalt modification applications [10]. On the one hand, nanoparticles have high surface energy and are prone to agglomeration, making uniform dispersion difficult. On the other hand, the mechanism of action of an individual material is relatively singular, making it difficult to simultaneously address the dual inhibition requirements of thermal-oxidative aging and UV aging. Therefore, overcoming the shortcomings of individual nanomaterials and achieving comprehensive improvement in anti-aging performance has become an urgent issue to be addressed.

To address the above problems, researchers have attempted to combine nanomaterials with different functions for composite modification. Among these, loading nano- TiO_2 or nano-CeO_2 onto the interlayer or surface of montmorillonite is a promising composite strategy, which can not only utilize the layered structure of montmorillonite to improve the dispersion of nanoparticles but also leverage the UV shielding or antioxidant functions of the nanoparticles to form a possible combined effect. In the field of asphalt modification, some researchers have applied CeO_2/MMT nanocomposites as a means to mitigate asphalt aging, and found that this composite could effectively prevent the rheological property decay of asphalt after aging [11, 12]. However, comparative studies on the anti-aging performance of different nanocomposite systems (e.g., MMT/TiO_2 and MMT/CeO_2) in asphalt are still lacking, and their distinct advantages under different aging modes (thermal-oxidative and ultraviolet) remain to be elucidated.

Therefore, this study further expands on the basis of the above research by preparing two types of multi-component nanocomposites using the sol-gel method: titanium dioxide/montmorillonite (TiO_2/MMT, abbreviated as TM) and cerium oxide/montmorillonite (CeO_2/MMT, abbreviated as CM). The corresponding modified asphalts (TMMA and CMMA) were prepared by melt blending and compared with base asphalt. Field emission scanning electron microscopy (FE-SEM) and ultraviolet-visible absorption spectroscopy (UV-Vis) were used to characterize the microstructure and optical properties of the nanocomposites. The RTFOT, PAV, and UV accelerated aging tests were employed to systematically evaluate the physical, rheological and chemical property changes of the two modified asphalts subjected to both thermo-oxidative and ultraviolet aging. The aim is to explore the improvement mechanism of TM and CM composites on the anti-aging performance of asphalt and compare their modification effects, providing a theoretical foundation and technical guidance for the

development of high-performance anti-aging asphalt.

2. Materials and test methods

2.1. Materials

The montmorillonite (MMT) used in this study was supplied by Zhejiang Fenghong New Materials Co., Ltd., and its basic properties are listed in Table 2. Titanium oxysulfate ($TiOSO_4$), cerium nitrate hexahydrate ($Ce(NO_3)_3 \cdot 6H_2O$), and citric acid were purchased from Aladdin. All chemicals were of analytical grade.

Table 3 lists the basic properties of the base asphalt supplied by Jiangsu Baoli Asphalt Co., Ltd. for this research.

2.2. Preparation methods of multi-component nanocomposites and their modified asphalts

The multi-component nanocomposites were prepared as follows: First, 1 mol of $TiOSO_4$ or $Ce(NO_3)_3 \cdot 6H_2O$ and 1 mol of citric acid were mixed in 50 mL of deionized water, followed by ultrasonic treatment for 0.5 h at room temperature. After aging for 24 h, MMT with a mass equal to that of $TiOSO_4$ or $Ce(NO_3)_3 \cdot 6H_2O$ was added under stirring. The mixture underwent magnetic stirring at 80°C for 2 h and then oven-dried at 100°C for 12 h. The obtained precursor was named P-TM or P-CM. The dried P-TM or P-CM specimens were transferred into a hightemperature furnace and ramped to 800°C at 5°C/min, then calcined for 10 h. The calcined samples were added to an ethanol solution and ball-milled for 5 h. The resultant solution was oven-dried at 100°C for 24 h, and the obtained solids were subsequently ground and sieved to yield the TM and CM multi-component nanocomposites. It should be noted that, although equal masses of the respective precursors and MMT were used, the final oxide loadings differ because of the different molar masses of the starting materials. Based on complete thermal conversion (1 mol precursor to 1 mol metal oxide), the theoretical final mass ratios are estimated to be approximately 0.50 (TiO_2/MMT) for the TM composite and approximately 0.40 (CeO_2/MMT) for the CM composite.

The multi-component nanocomposite modified asphalts were prepared as follows: First, base asphalt was oven-heated at 160 ± 5°C until it attained a molten state. After temperature equilibration, 0.5%, 1%, or 2% (by mass percentage of asphalt) of TM or CM modifier was incorporated into the molten asphalt. Subsequently, a high-speed shear emulsifier was employed to shear the asphalt samples at 4000 r/min and 160°C for 1 h to obtain titanium dioxide/montmorillonite nanocomposite modified asphalt and cerium oxide/montmorillonite nanocomposite modified asphalt, named TMMA and CMMA, respectively.

2.3. Test methods

The conventional physical property tests of asphalt mainly included penetration (25°C), ductility (10°C), and softening point. The specific test methods were as follows: The penetration test was measured according to the provisions of T0604 "Asphalt Penetration Test" in JTG 3410-2025 at a test temperature of 25°C. The softening point test was measured in line with the provisions of T0606 "Asphalt Softening Point Test" in JTG 3410-2025. The ductility test was measured according to the provisions of T0605 "Asphalt Ductility Test" in JTG 3410-2025. In this study, the test temperature was 10°C. Three replicate tests were conducted for penetration and ductility, and two for softening point.

The rheological properties of the modified asphalts were tested through an MCR-101 dynamic shear rheometer. According to the ASTM D7175 standard, the complex modulus (G*) of the asphalt specimens was obtained through a temperature sweep mode. The test conditions were set as follows: scanning frequency of 10 rad/s, strain of 1%, and temperature range of 30-90°C. Two replicate tests were conducted.

The ultraviolet-visible absorption spectrometer (UV-Vis Spectrophotometer) is a commonly used optical analysis instrument. The light absorption performance of MMT, TM, CM, nano- TiO_2, and nano- CeO_2 was analyzed by testing their absorption degree of ultraviolet light (200-400 nm) and visible light (400-800 nm).

The micro-morphology of MMT, TM, and CM was scanned using FE-SEM, revealing the bonding mode between nano-MMT and nano- TiO_2 or nano- CeO_2, thereby verifying whether the two nanomaterials were successfully composited.

The chemical structure of asphalt was analyzed by Attenuated total reflectance Fourier transform infrared (ATR-FTIR) spectroscopy. FTIR spectra were collected over a wavenumber range of $500 - 4000\ cm^{-1}$ at a resolution of $4\ cm^{-1}$, with 32 scans per sample. Sample preparation was carried out as follows: The asphalt sample is heated until fully molten, and a small aliquot is applied uniformly onto the ATR crystal to a thickness of about 1 mm , with care taken to avoid air bubbles and ensure good contact. The sample is then allowed to cool before scanning. Two replicate tests were conducted. At the chemical structure level, FTIR was used to track the evolution of characteristic functional groups during aging. In particular, the change in the carbonyl absorption peak at $1700\ cm^{-1}$ was of critical im-

Table 2. Basic properties of montmorillonite

Property	Value
Appearance	White or off-white fine powder
Loss on drying at 105°C	$\leq 3.5\%$
Fineness (passing 200-mesh)	$\geq 97\%$
Specific gravity (g/cm^3)	1.7
Bulk density (g/cm^3)	≤ 0.3

Table 3. Basic properties of 70# base asphalt

Technical Indicator	Value
Penetration (25°C, 0.1 mm)	61.0
Softening point (°C)	48.4
Ductility (15°C)	>150
Brookfield viscosity (135°C, mPa•s)	456

portance. Therefore, the carbonyl index (CI) was adopted as the chemical indicator for evaluating the anti-aging performance of asphalt. In order to accurately calculate CI according to the equation 1, prior to integration, all spectra underwent baseline correction using a two-point linear baseline method. Specifically, two baseline points were selected on the relatively flat absorption valleys on both sides of the target peak, and a straight line connecting these two points was constructed as the baseline. To eliminate variations in sample thickness and contact pressure, all spectra were normalized using the area under the reference peak corresponding to the C-H stretching vibration (centered at 1376 cm^{-1}) before calculating the indices. It should be emphasized that the integration ranges for the carbonyl band were not fixed at predetermined, constant wavenumber intervals. Instead, we employed a two-point tangent method to determine the integration limits. For each spectrum, two tangential baseline points were selected on the shoulders of the carbonyl absorption band. The baseline was then constructed by connecting these two points, and the intersection points of this tangent line with the peak profile were used as the exact lower and upper integration boundaries for the carbonyl band. Similarly, for the reference band at 1376 cm^{-1}, the integration limits were also determined dynamically using the same two-point tangent approach. This dynamic integration strategy ensures that the calculated indices objectively accommodate minor peak-shape variations caused by different aging degrees, rather than introducing artificial errors from fixed integration windows.

$$\mathrm{CI} = \frac{\text{Area of carbonyl band centered around } 1700\ \mathrm{cm}^{-1}}{\text{Area of } CH_3 \text{ umbrella vibration centered around } 1376\ \mathrm{cm}^{-1}} \tag{1}$$

In this research, the thermal-oxidative aging simulation tests of asphalt were conducted according to the provisions of T0610 "Asphalt Rolling Thin Film Oven Aging Test (RTFOT Method)" and T0630 "Asphalt Heating Aging Test (PAV Method)" in JTG 3410-2025. Meanwhile, the ultraviolet aging test was realized using a self-built UV accelerated aging system, which consisted of a 500 W high-pressure mercury lamp (8 W/m^2 irradiance) and a constant temperature chamber $(60 \pm 2°C)$ [**13**, 13–15]. The specimens were placed 45 cm away from the UV source and subjected to continuous ultraviolet irradiation for 6 days.

2.4. Aging evaluation indicators

The main aging evaluation indicators used in this study included softening point increment (SPI), retained penetration (RP), ductility retained rate (DRR), complex modulus aging index (CMAI), and carbonyl index increment (ΔCI). The specific calculation formulas are as follows. Generally, the more severe the aging, the higher the SPI, CMAI and ΔCI, while the lower the RP and DRR.

$$\begin{aligned}\mathrm{SPI}\,(°\mathrm{C}) = {} & \text{Softening point after aging} \\ & - \text{Softening point before aging}\end{aligned} \tag{2}$$

$$\mathrm{RP}\,(\%) = \frac{\text{Penetration after aging}}{\text{Penetration before aging}} \times 100 \tag{3}$$

$$\mathrm{DRR}\,(\%) = \frac{\text{Ductility after aging}}{\text{Ductility before aging}} \times 100 \tag{4}$$

$$\mathrm{CMAI} = \frac{\text{Complex modulus after aging}}{\text{Complex modulus before aging}} \tag{5}$$

$$\Delta\mathrm{CI} = \mathrm{CI}_{\text{after aging}} - \mathrm{CI}_{\text{before aging}} \tag{6}$$

3. Results and discussion

3.1. UV-Vis absorption ability analysis of multi-component nanocomposites

To investigate the UV shielding performance of the two multi-component nanocomposites, TM and CM, this study used a UV-Vis absorption spectrometer to measure their absorbance in the wavelength range of 220 − 480 nm, and compared them with pure MMT, nano- TiO_2, and nano- CeO_2. As depicted in Fig. 1, the absorption spectra of different materials exhibit substantial differences in the UV region and visible light region. Individual nano- TiO_2 and nano- CeO_2 exhibited the highest absorbance in the UV region, indicating their optimal UV absorption efficiency. The absorbance of the TM composite was slightly lower than that of the two individual nanoparticles but still close to them, and pronouncedly higher than that of pure MMT, indicating that TM successfully retained the UV absorption characteristics of nano- TiO_2. The absorbance of the CM composite was markedly lower than that of TM and the two individual nanoparticles, only slightly higher than that of pure MMT, suggesting its relatively limited UV absorption capacity, which may be related to the loading effect of CeO_2 on the MMT surface. Pure MMT exhibited the lowest absorbance and is difficult to use alone as a UV shielding material.

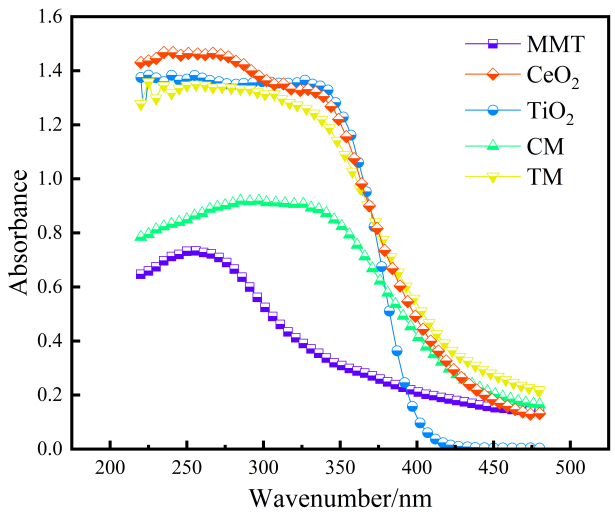


Fig. 1. UV-Vis spectra of multi-component nanocomposites

3.2. Surface microstructure analysis of multi-component nanocomposites

To observe the surface morphology and nanoparticle loading status of the two multicomponent nanocomposites, TM and CM, this study characterized their microstructures using FE-SEM. As presented in Fig. 2(a), MMT exhibits a typical layered structure with a flat and smooth surface and relatively large particle size, providing sufficient loading area. Fig. 2(b) shows the FE-SEM image of the CM composite. Nano-CeO2 particles are loaded on the MMT surface, but agglomeration can be observed in some areas, and the overall distribution uniformity is relatively poor. Fig. 2(c) presents the FE-SEM image of the TM composite. The originally smooth MMT surface becomes rough, and a large number of nano-sized particles are uniformly attached, indicating that nano- TiO_2 has been successfully loaded onto the MMT surface, forming a structurally stable multi-component nanocomposite. This difference in microstructure is consistent with the conclusion from Section 3.1 that TM exhibits better UV absorption capacity than CM, indicating that uniform loading of nanoparticles on the MMT surface is an important contributory factor to achieving excellent UV shielding performance, although other factors such as differences in oxide content and particle characteristics may also be involved.

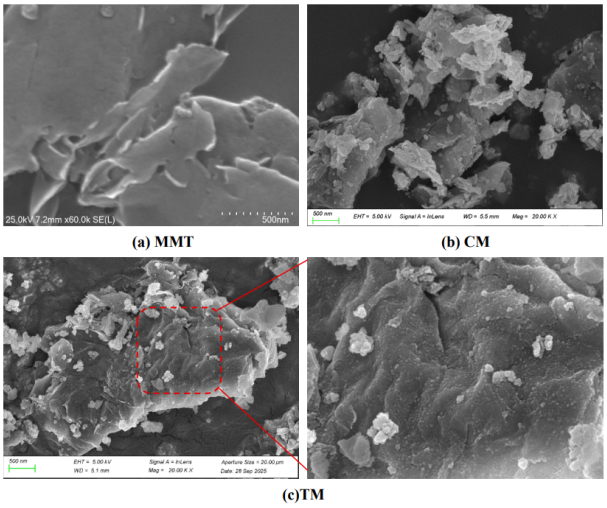


Fig. 2. FE-SEM images of multi-component nanocomposites

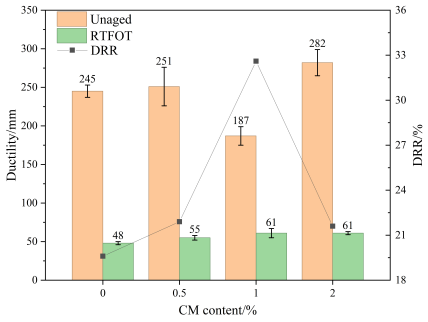
3.3. Effect of multi-component nanocomposites on physical properties of asphalt after RTFOT aging

Fig. 3 shows the ductility data of different asphalts at 10°C before and after RTFOT aging. Before aging, the effect of different multi-component nanocomposite dosages on the ductility of asphalt varied. For CMMA, at dosages of 0.5% and 2%, the unaged ductility values were 251 mm and 282 mm , respectively, both higher than that of base asphalt (245 mm); while at a dosage of 1%, the unaged ductility

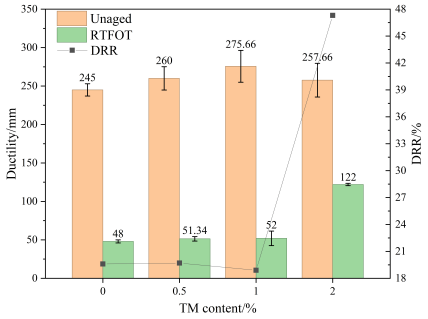
decreased to 187 mm, which was lower than that of base asphalt. For TMMA, the unaged ductility values at the three dosages were 260 mm, 275.7 mm, and 257.7 mm, respectively, all bigger than that of base asphalt, manifesting that the addition of TM composite has no substantial adverse influence on the ductility of asphalt. After

RTFOT aging, the ductility of all asphalts decreased to varying degrees. The ductility of base asphalt decreased to 48 mm, with a DRR of 19.6%. For CMMA at dosages of 0.5%, 1%, and 2%, the DRRs after aging were 21.9%, 32.6%, and 21.6%, respectively. Notably, the CMMA ductility exhibits a non-monotonic dependence on dosage. This is likely because at 1%, CM disrupts the asphalt molecular network [12], reducing unaged ductility; at 2%, however, it may form a more continuous structure that better accommodates deformation. Regarding DRR, it is a relative index and is lower at 2% mainly because of its much higher baseline; the absolute ductility after aging at 2%(61 mm) is identical to that at 1% and considerably bigger than that of base asphalt (48 mm), confirming effective aging resistance at both dosages. For TMMA at dosages of 0.5%, 1%, and 2%, the DRRs after aging were 19.7%, 18.9%, and 47.3%, respectively. In terms of DRR, TMMA showed particularly outstanding performance at a dosage of 2%, much higher than that of other asphalts. It is worth noting that the ductility of 2% TMMA after aging was still as high as 122 mm, indicating that it maintains good lowtemperature ductility after RTFOT aging, demonstrating an observable effect in resisting shortterm thermal-oxidative aging. This is attributed to the layered structure of MMT, which can form a physical barrier in asphalt, delaying oxygen penetration and the evaporation of light fractions, thereby inhibiting the thermal-oxidative aging process of asphalt [9]. At the same time, the introduction of nano- TiO_2 and nano- CeO_2 may further retard aging through their antioxidant properties. When the TM dosage reaches 2%, the physical barrier effect of MMT and the antioxidant influence of nano- TiO_2 form a possible combined effect, effectively inhibiting the thermal oxidation of asphalt, thus maintaining a high DRR.

Fig. 4 shows the penetration test results of different asphalts at 25°C before and after RTFOT aging. With the dosage increasing, the penetration values of both CMMA and TMMA before aging initially rose and subsequently declined. When the dosage increased from 0% to 1%, the penetration of both modified asphalts increased markedly. Specifically, the penetration of 1% CMMA increased by 28.0% compared with base asphalt, and that of 1% TMMA increased by 13.7%. This indicates that incorporating an appropriate amount of nanocomposites lowers the consistency of asphalt, possibly owing to the lubrication effect of



(a) CMMA

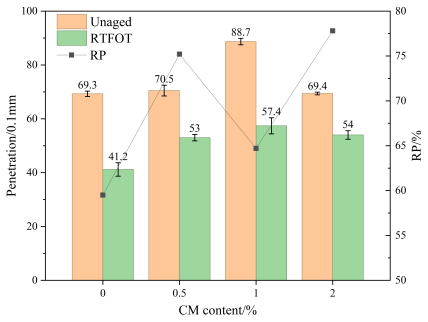


(b) TMA

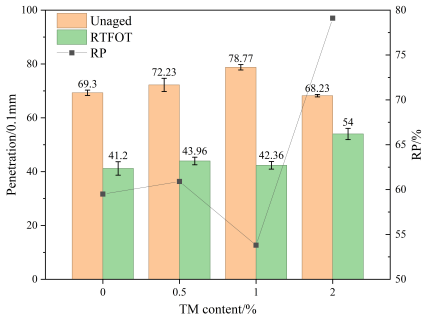
Fig. 3. Effect of multi-component nanocomposites on the ductility of asphalt before and after RTFOT aging

nano- TiO_2 and nano- CeO_2 particles in asphalt. However, when the dosage further increased to 2%, the penetration of both modified asphalts decreased to a level resembling that of base asphalt. This may be because the layered structure of montmorillonite begins to dominate at higher dosages, and its rigid characteristics offset the lubrication effect of the nanoparticles. In addition, after RTFOT aging, the penetration of all asphalts decreased to varying degrees. The penetration of base asphalt decreased to 41.2 dmm after aging, with a RP of only 59.5%. Although the RP of CMMA modified asphalt did not show an obvious trend with dosage variation, it was pronouncedly higher than that of base asphalt for all dosages, reaching 77.8% at a dosage of 2%. For TMMA modified asphalt, when the dosage did not exceed 1%, the RP showed little change, but it substantially increased to 79.2% when the dosage reached 2%. Both multi-component nanocomposites exhibited the highest RP at a dosage of 2%. Analyzing the reasons, the layered structure of MMT can form a physical barrier in asphalt, delaying oxygen penetration and the volatilization of light components. When the composite dosage reaches 2%, the physical barrier effect of MMT dominates, while the antioxidant properties of nano- TiO_2 and nano- CeO_2 provide complementary protection, effectively inhibiting

the oxidative hardening of asphalt, thus maintaining a high RP. At lower dosages (0.5%-1%), the softening effect of nanoparticles is more prominent, but the barrier network of montmorillonite has not yet been effectively formed, resulting in relatively unstable anti-aging performance.



(a) CMMA

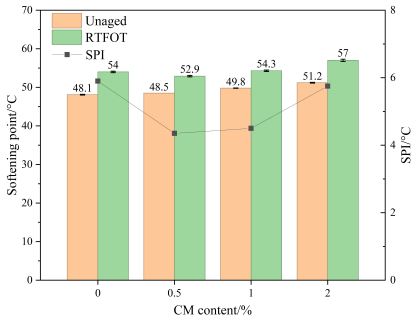


(b) TMA

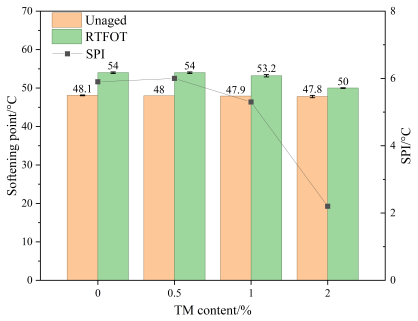
Fig. 4. Effect of multi-component nanocomposites on penetration of asphalt before and after RTFOT aging

Fig. 5 presents the softening point data of different asphalt specimens pre- and post-RTFOT aging. Fig. 5 reveals that the base asphalt had a softening point of 48.1°C prior to aging. The softening point of CMMA modified asphalt rose progressively with increasing dosage: at dosages of 0.5%, 1%, and 2%, the softening points were 48.5°C, 49.8°C, and 51.2°C, respectively, all slightly higher than that of base asphalt, suggesting that incorporating CM composite can enhance the high-temperature performance of asphalt to some degree, which may be related to the rigid layered structure of montmorillonite. The softening point of TMMA modified asphalt marginally decreased with increasing dosage: at dosages of 0.5%, 1%, and 2%, the softening points were 48.0°C, 47.9°C, and 47.8°C, respectively, which were basically the same as or slightly lower than that of base asphalt, manifesting that the TM composite does not considerably affect on the high-temperature performance of asphalt.

After RTFOT aging, the softening point of base asphalt rose to 54.0°C, with a SPI of 5.9°C. For CMMA at dosages of 0.5%, 1%, and 2%, the SPIs were 4.4°C, 4.5°C, and 5.8°C, respectively. At dosages of 0.5% and 1%, the SPIs were smaller than that of base asphalt, while at a dosage of 2%, the SPI was comparable to that of base asphalt. For TMMA at dosages of 0.5%, 1%, and 2%, the SPIs were 6.0°C, 5°3°C, and 2.2°C, respectively, among which 2% TMMA exhibited the smallest SPI.



(a) CMMA



(b) TMA

Fig. 5. Effect of multi-component nanocomposites on softening point of asphalt before and after RTFOT aging

In summary, the addition of multi-component nanocomposites markedly influences the performance of asphalt prior to and following short-term thermal-oxidative aging. Among them, 2% TMMA exhibited better performance than base asphalt and modified asphalts with other dosages in terms of DRR, RP, and SPI, while 2% CMMA also demonstrated a certain antiaging ability. Considering that the physical barrier network of the nanocomposites has not been fully formed at lower dosages, resulting in unstable anti-aging performance, 2% TMMA and 2% CMMA were selected as representative samples to further investigate their physical and rheological property evolution under long-term aging (PAV and UV) conditions, so as to comprehensively assess the anti-aging ability of the two multi-component nanocomposites.

3.4. Effect of multi-component nanocomposites on physical and rheological properties of asphalt after long-term aging

Fig. 6 shows the softening point data of different asphalts before and after long-term aging (PAV and UV). After PAV aging, the SPI of base asphalt was 15.2°C, indicating notably hardening after long-term aging. The SPIs of 2% CMMA and 2% TMMA were 13.4°C and 12.8°C, separately, both lower than that of base asphalt. Both modified asphalts effectively inhibited hardening during the long-term thermal-oxidative aging process, with 2% TMMA exhibiting a slightly lower SPI than 2% CMMA, demonstrating superior resistance to long-term thermal-oxidative aging. This is attributed to the possible combined effect of the layered physical barrier of montmorillonite and the antioxidant properties of nano- TiO_2, which effectively retards the deep oxidation of asphalt [11].

In addition, Fig. 6 shows that after UV aging, the SPI of base asphalt was at a relatively high level, indicating its lack of an effective light shielding mechanism. The UV aging softening point increment of 2% TMMA was markedly lower than that of 2% CMMA, demonstrating superior resistance to photo-oxidative aging. Based on the microstructure analysis in Fig. 2, nano- TiO_2 in the TM system exhibits more uniform and dense loading on the MMT surface compared with the CM system. This morphological feature is likely associated with a more continuous physical shielding configuration within the asphalt, which may contribute to reducing the penetration depth of ultraviolet light. This could partially explain the better UV aging protection capability observed for the TMMA sample.

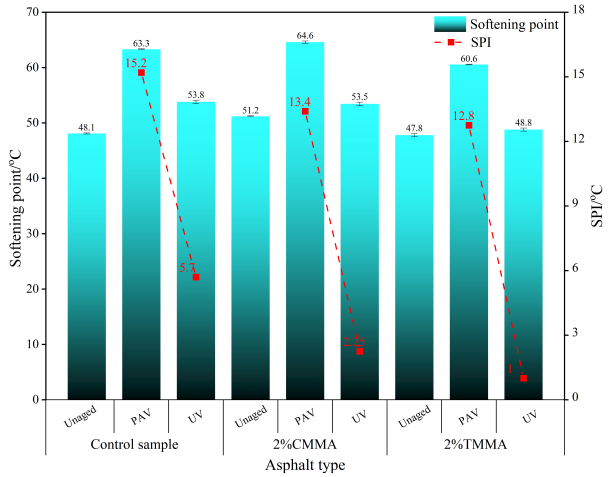
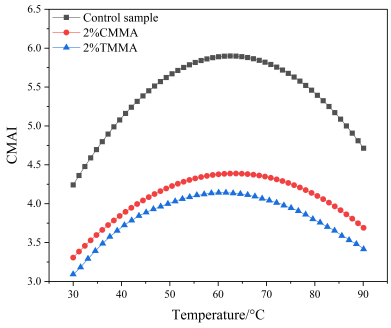


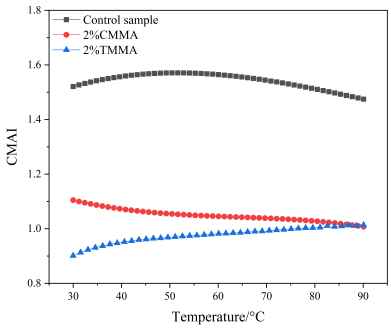
Fig. 6. Effect of multi-component nanocomposites on softening point of asphalt before and after long-term aging

The CMAI reflects the degree of stiffness increase of asphalt after aging. A larger CMAI value indicates a more severe increase in stiffness after aging. Fig. 7(a) displays the CMAI curves of different asphalts as a function of temperature after PAV aging. Over the entire temperature range, the base asphalt showed the highest CMAI values, manifesting a severe modulus increase after long-term thermal-oxidative aging. The CMAI curves of 2% CMMA and 2% TMMA were both notably shifted downward, with 2% TMMA showing lower CMAI values than 2% CMMA, indicating its better performance in inhibiting rheological modulus increase. This observation is consistent with the more uniform nanoparticle dispersion in TM (Fig. 2), which may contribute, along with other factors such as oxide content and particle characteristics, to enhanced barrier protection against oxygen penetration.

Fig. 7(b) presents the CMAI curves of different asphalts as a function of temperature after UV aging. The CMAI of base asphalt was markedly higher than that of modified asphalts over the entire temperature range, and 2% TMMA was superior to 2% CMMA in inhibiting modulus increase. According to the UV absorption spectrum in Fig. 1, TM exhibited higher absorbance than CM in the UV region, indicating its better UV shielding capability.



(a) PAV

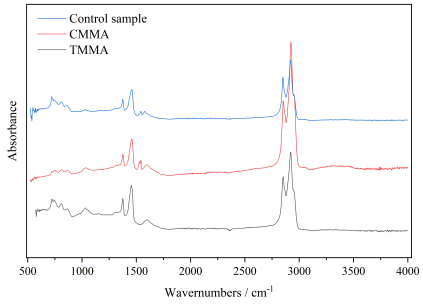


(b) UV

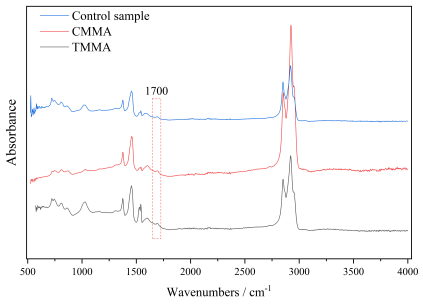
Fig. 7. Effect of multi-component nanocomposites on rheological properties of asphalt before and after different long-term aging conditions

3.5. Effect of multi-component nanocomposites on chemical structure of asphalt after long-term aging

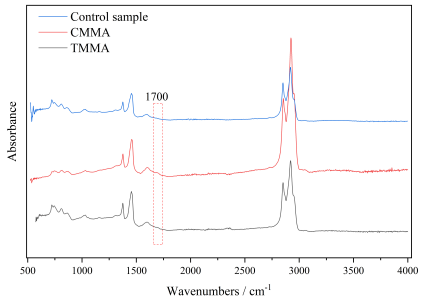
Fig. 8a presents the FTIR results of different asphalts before and after different longterm aging conditions. The corresponding carbonyl index (CI) and carbonyl index increment (ΔCI) are shown in Fig. 9. Compared with the control sample, both CMMA and TMMA exhibit lower ΔCI values under both PAV and UV aging conditions, indicating that the multicomponent nanocomposites effectively inhibit the oxidative aging of asphalt, with TM showing a more obvious effect. This finding is consistent with the previously observed results of SPI and CMAI.



(a) Unaged

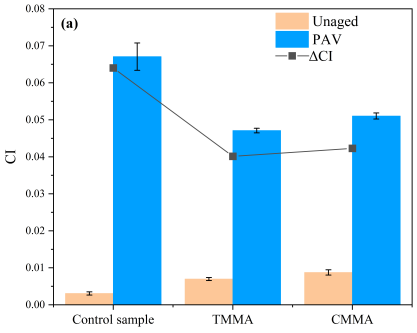


(b) PAV

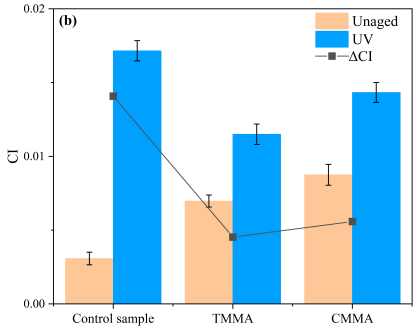


(c) TM

Fig. 8. FTIR results of different asphalts before and after different long-term aging conditions: (a) Unaged, (b) PV, and (c) UV



(a) PAV



(b) UV

Fig. 9. CI and **ΔCI** results of different asphalts before and after different long-term aging conditions

4. Conclusions

In this study, two multi-component nanocomposites, TM and CM, were successfully prepared using the sol-gel method. The microstructure and optical properties of the nanocomposites were characterized by FE-SEM and UV-Vis spectroscopy. The physical and rheological property changes of the two modified asphalts subjected to thermal-oxidative and UV aging were systematically assessed through RTFOT, PAV, and UV accelerated aging tests. The main findings are as follows:

(1) Two multi-component nanocomposites, TM and CM, were successfully synthesized via the sol-gel route. FE-SEM characterization revealed that nano-TiO_2 in TM was uniformly dispersed and loaded onto the MMT surface, whereas nano-CeO_2 in CM exhibited agglomeration and poor spatial distribution. UV-Vis analysis indicated that the UV absorbance of TM was markedly higher than that of CM, aligning with microstructural observations and demonstrating that uniform nanoparticle dispersion, alongside intrinsic oxide characteristics and loading content, critically enhances UV shielding performance.

(2) Prior to aging, incorporating an optimal dosage of

multi-component nanocomposites improved both the low-temperature ductility and consistency of the asphalt binder; however, the extent of modification depended heavily on modifier type and concentration. Following RTFOT aging, 2% TMMA demonstrated significantly higher DRR and RP alongside a substantially lower SPI compared to base asphalt, confirming superior resistance to short-term thermal-oxidative aging.

(3) Following either PAV or UV accelerated aging, 2% TMMA consistently exhibited lower SPI, CMAI, and ΔCI values than 2% CMMA, demonstrating enhanced inhibition against long-term thermal-oxidative and UV-induced degradation. These macroscopic aging trends closely corroborate the microstructural dispersion and UV-shielding advantages identified via FE-SEM and UV-Vis analyses.

(4) Comprehensive physical, rheological, and chemical evaluations confirmed that both TM and CM effectively mitigate asphalt aging through synergistic mechanisms: the tortuous physical barrier provided by layered montmorillonite platelets combined with the UV-shielding and antioxidant activities of nano-TiO_2 or nano-CeO_2. Among all formulations, 2% TMMA exhibited optimal aging resistance across all conditioning regimes at the binder scale. Nevertheless, mixture-level mechanical evaluations and long-term field validation remain essential prior to correlating these laboratory binder metrics directly with pavement service life.

Acknowledgments

This work was supported by Hunan Provincial Natural Science Foundation of China (grant number 2026JJ90005), the Scientific Research Project of Hunan Provincial Education Department (grant numbers 24B0188). The authors gratefully acknowledge their financial support.

References

[1] Y. Gao, D. Geng, X. Huang, and G. Li, (2017) *"Degradation evaluation index of asphalt pavement based on mechanical performance of asphalt mixture"* **CONSTRUCTION AND BUILDING MATERIALS *140***: 75–81. DOI: 10.1016/j.conbuildmat.2017.02.095.

[2] S. Yang, H. Park, and C. Baek, (2023) *"Fatigue Cracking Characteristics of Asphalt Pavement Structure under Aging and Moisture Damage"* **SUSTAINABILITY *15***(6): DOI: 10.3390/su15064815.

[3] R. Tauste, F. Moreno-Navarro, M. Sol-Sanchez, and M. C. Rubio-Gamez, (2018) *"Understanding the bitumen ageing phenomenon: A review"* **CONSTRUCTION AND BUILDING MATERIALS *192***: 593–609. DOI: 10.1016/j.conbuildmat.2018.10.169.

[4] R. Polo-Mendoza, G. Martinez-Arguelles, L. F. Walubita, F. Moreno-Navarro, F. Giustozzi, L. Fuentes, and T. Navarro-Donado, (2022) *"Ultraviolet ageing of bituminous materials: A comprehensive literature review from 2011 to 2022"* **CONSTRUCTION AND BUILDING MATERIALS *350***: DOI: 10.1016/j.conbuildmat.2022.128889.

[5] I. G. d. N. Camargo, T. Ben Dhia, A. Loulizi, B. Hofko, and J. Mirwald, (2021) *"Anti-aging additives: proposed evaluation process based on literature review"* **ROAD MATERIALS AND PAVEMENT DESIGN *22***(1, SI): S134–S153. DOI: 10.1080/14680629.2021.1906738.

[6] Z. Feng, F. Cai, D. Yao, and X. Li, (2021) *"Aging properties of ultraviolet absorber/SBS modified bitumen based on FTIR analysis"* **CONSTRUCTION AND BUILDING MATERIALS *273***: DOI: 10.1016/j.conbuildmat.2020.121713.

[7] S. Li, X. Zhang, Y. Shi, C. Yan, and S. Zhou, (2023) *"Synergistic Effect and Mechanism of Nanomaterial Compounded with Sustainable Lignin for Aging Resistance of Asphalt"* **ACS SUSTAINABLE CHEMISTRY & ENGINEERING *11***(33): 12304–12316. DOI: 10.1021/acssuschemeng.3c02078.

[8] J. Li, X. Ye, Y. Zhao, D. Yang, D. Li, C. Han, and X. Li, (2023) *"Structure-performance evolution on thermal-oxidative aging of CeO2/SBS co-modified asphalt"* **INTERNATIONAL JOURNAL OF PAVEMENT ENGINEERING *24***(2): DOI: 10.1080/10298436.2022.2111425.

[9] H. L. Zhang, J. Y. Yu, and D. L. Kuang, (2013) *"The Effect of Sodium and Organic Montmorillonites on the Thermal Aging Properties of Bitumen"* **PETROLEUM SCIENCE AND TECHNOLOGY *31***(20): 2074–2081. DOI: 10.1080/10916466.2012.678538.

[10] H. Zhang, H. Duan, C. Zhu, Z. Chen, and H. Luo, (2021) *"Mini-Review on the Application of Nanomaterials in Improving Anti-Aging Properties of Asphalt"* **ENERGY & FUELS *35***(14): 11017–11036. DOI: 10.1021/acs.energyfuels.1c01035.

[11] C. Zhu, Z. Sun, F. Xu, H. Zhang, and X. Guo, (2025) *"Protection effect for polymer-in rich phase in SBS modified asphalt during long-term aging by different*

MMT/TiO2/SBS pretreatment methods" **FUEL *400***: DOI: 10.1016/j.fuel.2025.135802.

[12] C. Zhu, Z. Xu, H. Zhang, Z. Wang, D. Li, N. Su, and D. Zhang, (2025) *"Rheological and micro characteristics of asphalt containing different nanocomposite ratios of CeO2/MMT during thermal-oxidative and ultraviolet aging"* **CONSTRUCTION AND BUILDING MATERIALS *495***: DOI: 10.1016/j.conbuildmat.2025.143732.

[13] Z. Feng, J. Yu, L. Xue, and Y. Sun, (2013) *"Rheological and aging properties of ultraviolet absorber/styrenebutadienestyrenemodified bitumens"* **JOURNAL OF APPLIED POLYMER SCIENCE *128***(4, SI): 2571–2577. DOI: 10.1002/app.38505.

[14] H. Wu, L. Li, J. Yu, S. Xu, and D. Xie, (2016) *"Effect of layered double hydroxides on ultraviolet aging properties of different bitumens"* **CONSTRUCTION AND BUILDING MATERIALS *111***: 565–570. DOI: 10.1016/j.conbuildmat.2016.02.140.

[15] H. Liu, Z. Zhang, J. Xie, Z. Gui, N. Li, and Y. Xu, (2021) *"Analysis of OMMT strengthened UV aging-resistance of Sasobit/SBS modified asphalt: Its preparation, characterization and mechanism"* **JOURNAL OF CLEANER PRODUCTION *315***: DOI: 10.1016/j.jclepro.2021.128139.